Elements of the Dynamical Response to Climate Change over the Mediterranean

ALEXANDRE TUEL,[a,c] PAUL A. O'GORMAN,[b] AND ELFATIH A. B. ELTAHIR[a]

[a] *Ralph M. Parsons Laboratory, Massachusetts Institute of Technology, Cambridge, Massachusetts*
[b] *Department of Earth, Atmospheric, and Planetary Sciences, Massachusetts Institute of Technology, Cambridge, Massachusetts*

(Manuscript received 5 June 2020, in final form 16 October 2020)

ABSTRACT: Future climate simulations indicate that the Mediterranean Basin will experience large low-level circulation changes during winter, characterized by a strong anomalous ridge that drives a regional precipitation decline. Previous research highlighted how shifts in stationary wave structure and the atmospheric response to reduced warming of the Mediterranean Sea relative to land could explain the development of this anomalous pressure high. Here, we expand on these results and provide new arguments for why and how the Mediterranean is projected to experience large circulation changes during winter. First, we find that zonal asymmetries in the vertical structure of stationary waves are important to explain the enhanced circulation response in the region and that these asymmetries are related through the external mode to the vertical structure of the mean zonal wind. Second, in winter, the Mediterranean is located just to the north of the Hadley cell edge and consequently is relatively free of large-scale descent; together with low near-surface static stability above the sea, this condition allows the weaker warming trend above the sea to propagate to the low troposphere and trigger a major circulation response. During summer, however, remotely forced descent and strong static stability prevent the cooling anomaly from expanding upward. Most of the intermodel scatter in the projected low-level circulation response in winter is related to the spread in upper-tropospheric dynamical trends. Importantly, because climate models exhibit too much vertical coherence over the Mediterranean, they likely overestimate the sensitivity of Mediterranean near-surface circulation to large-scale dynamical changes.

KEYWORDS: Mediterranean Sea; Atmospheric circulation; Rossby waves; Stationary waves; Atmosphere-ocean interaction; Climate change

1. Introduction

The Mediterranean Basin (30°–45°N, 10°W–40°E) has stood out in successive generations of climate models as one of the few regions where circulation projections are particularly robust. In particular, a large majority of models in both CMIP3 and CMIP5 agree on the development of an anomalous pressure high during winter (Giorgi and Lionello 2008; Seager et al. 2014), whose magnitude largely surpasses that of changes elsewhere in the Northern Hemisphere (Fig. 1). Changes in regional winter circulation have long been suspected to drive the projected decrease in the frequency of Mediterranean cyclones and the concurrent regional precipitation decline (Zappa and Shepherd 2017). North African wind anomalies were shown to be strongly related to regional precipitation anomalies and explained most of the latter's scatter across CMIP5 models (Zappa et al. 2015). Regional circulation trends were subsequently linked to large-scale dynamics (Seager et al. 2019; Brogli et al. 2019; Tuel and Eltahir 2020) and the land-sea warming contrast (Brogli et al. 2019; Tuel and Eltahir 2020). Tuel and Eltahir (2020, hereinafter TE20) explained the development of the anomalous Mediterranean high as the combined response to shifts in the large-scale structure of the mean wintertime circulation and to surface temperature trends. A robust eastward shift in winter stationary waves (Simpson et al. 2016) pushes the Atlantic Ocean subtropical high closer to the Mediterranean Sea while the relative cooling of Mediterranean sea surface temperatures (SSTs) in comparison with the surrounding land triggers higher pressure over the eastern part of the basin. The link between circulation and precipitation trends was discussed by TE20, who showed how the strong wind anomalies associated with the increase in surface pressure suppressed precipitation at each end of the basin.

Although we now have a good understanding that both shifts in stationary waves and relative cooling of SSTs contribute to the lower-tropospheric anticyclonic anomaly, two important dynamical aspects of the response remain unclear and are addressed in this paper. First, the upper-level changes in circulation have been explained in terms of changes in stationary wave propagation and are of similar magnitude across longitudes, but it is the lower-level circulation response that is most important for changes in precipitation. Why is the low-level response to the stationary wave changes particularly large in the Mediterranean as shown usinga statistical approach in TE20? Furthermore, is the link between upper- and lower-level circulation changes consistent with stationary-wave theory, and is it well represented in climate models? Second, the relative cooling of the Mediterranean SSTs occurs both in summer and winter, but the anomalous high pressure only occurs in winter. Why does the response to relative cooling of the Mediterranean Sea lead to a large dynamical response in winter and not in summer? Section 2 of this paper presents the data used for analysis. In section 3, we analyze the connection between circulation changes in the upper and lower troposphere from the perspective of the external mode—the dominant mode in the vertical

Supplemental information related to this paper is available at the Journals Online website: https://doi.org/10.1175/JCLI-D-20-0429.s1.

[c] Current affiliation: Institute of Geography, Oeschger Centre for Climate Change Research, University of Bern, Bern, Switzerland.

Corresponding author: A. Tuel, atuel@alum.mit.edu

DOI: 10.1175/JCLI-D-20-0429.1

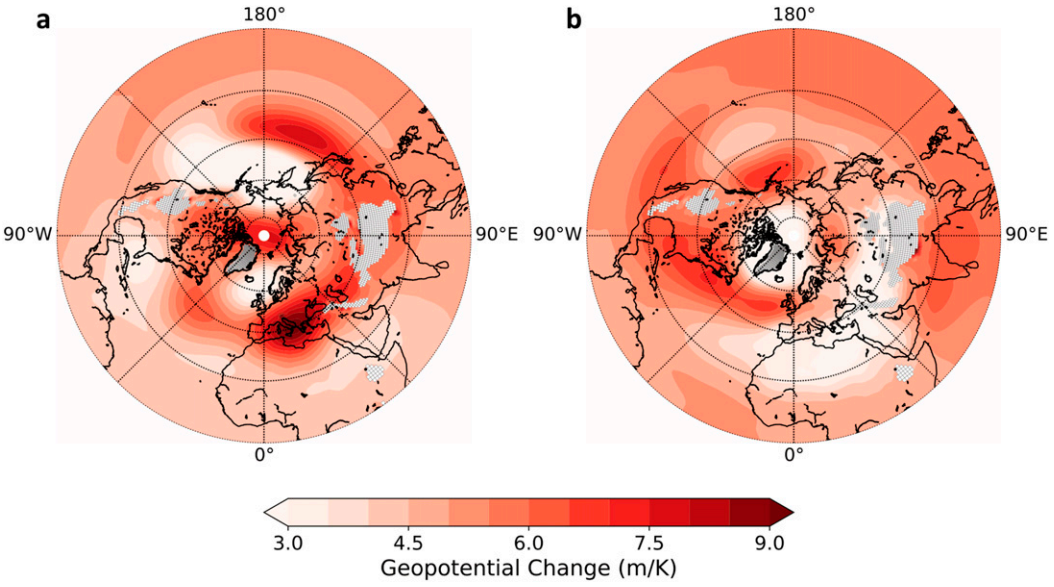

FIG. 1. CMIP5 multimodel mean change (2071–2100 minus 1976–2005) in (a) DJF and (b) JJA 850-hPa geopotential height, normalized by each model's global-mean projected temperature change. Gray hatching indicates areas where the 850-hPa level is below the surface.

structure of midlatitude flow—estimated using the quasi-geostrophic approximation. We show that the structure of the external mode varies significantly with longitude and modulates low-level circulation trends in a way that amplifies the response over the Mediterranean. Then, in section 4, we turn to the impact of relative SST cooling with respect to land and contrast the winter and summer response using regional climate simulations. We end in section 5 with an additional discussion and our conclusions.

2. Data

As estimate of the current climate, we consider the ERA-Interim reanalysis (Dee et al. 2011) over the 1979–2018 period. ERA-Interim is based on an atmospheric model and reanalysis system with a horizontal grid spacing of about 79 km. Here, we perform our calculations with data archived on a regular 1° grid with 17 pressure levels at monthly resolution. We also analyze global climate model (GCM) output from 28 models of phase 5 of the Coupled Model Intercomparison Project (CMIP5; Taylor et al. 2012) under the historical and RCP8.5 scenarios, and 11 models from the Atmospheric Model Intercomparison Project (AMIP; Gates et al. 1999), under the "amip" and "amipFuture" scenarios. In amip, the atmosphere is forced by observed time-varying SSTs and sea ice at present-day atmospheric composition, while a patterned SST anomaly is added in the amipFuture runs (sea ice and CO_2 being kept the same). The SST pattern is based on the CMIP3 multimodel-mean SST response to a quadrupling of CO2, where individual CMIP3 model responses are normalized to have a global-mean 4-K warming (see details at https://www.earthsystemcog.org/projects/cfmip/cfmip2-cmip5). The list of models is given in Tables S1 and S2 in the online supplemental material. For the CMIP models, we use as reference the 1976–2005 period in the historical runs, and the 2071–2100 period under RCP8.5 for long-term projections. For AMIP, the amip and amipFuture runs both cover the same period, usually 1979–2008, but with some variability across models (see Table S2). For runs longer than 30 years, we keep only the last 30 years for analysis; otherwise, all available years are retained. The amip runs are used as reference. Our analysis also relies on output from the regional climate simulations developed in TE20 using the MIT Regional Climate Model. TE20 ran two sets of simulations over a domain covering the Mediterranean Sea and most of Europe: one forced with ERA-Interim data as boundary conditions over the 1981–2011 period ("ERA"), and one forced with output from the MPI-ESM-MR model (Zanchettin et al. 2013) under the RCP8.5 scenario between 2070 and 2100 ("MPI"). Each set comprises a reference (unperturbed) run (designated by "0C"), and a perturbed run in which Mediterranean SSTs are uniformly warmed by 1.5°C year-round (designated by "+1.5°C"). The +1.5°C perturbed experiment is designed to "cancel out" the future wintertime relative cooling of the Mediterranean with respect to the surrounding land projected by CMIP5 models (TE20). Thus, this framework allows one to estimate the impact of the relative SST cooling on the regional climate by taking the difference between the +1.5°C and 0°C simulations.

3. Large-scale dynamics

a. Changes in stationary planetary waves

Wintertime midlatitude flow in the Northern Hemisphere is strongly modulated by atmospheric stationary waves, which arise from orographic and atmospheric diabatic forcing, land–sea thermal contrasts, as well as transient eddy heat and momentum fluxes (Hoskins and Karoly 1981; Held et al. 2002). Stationary waves exhibit wavelengths ranging roughly from a few thousand to twenty thousand kilometers, and generate large-scale variations in the

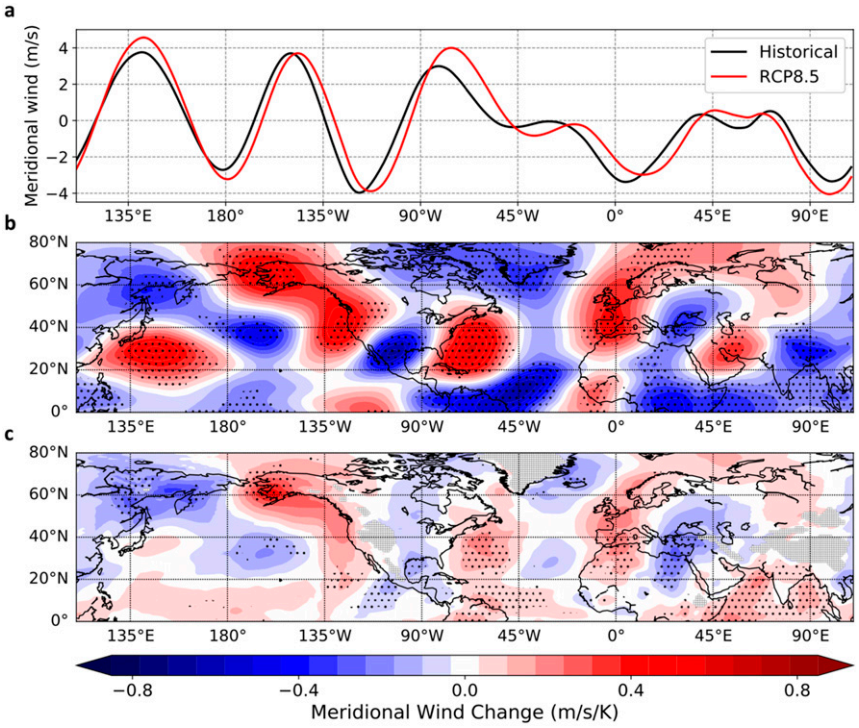

FIG. 2. (a) CMIP5 multimodel mean 300-hPa meridional winds in DJF in the historical and RCP8.5 scenarios, averaged between 20° and 50°N. Also shown are CMIP5 multimodel mean projected change in DJF meridional winds at (b) 300 and (c) 850 hPa. Gray hatching in (c) indicates areas where the 850-hPa level is below the surface. For each model, projections were normalized by its mean annual global temperature change. Stippling indicates that more than 80% of models agree on the sign of the change.

atmospheric circulation, leading to large longitudinal asymmetries in the distribution of temperature and precipitation. Global climate models robustly agree on the pattern of change in upper-tropospheric wintertime circulation in the Northern Hemisphere (Simpson et al. 2016; Wills et al. 2019), consisting of a strengthened jet stream and alternating cyclonic and anticyclonic circulation anomalies between 20° and 60°N. The acceleration of the jet stream follows from the thermal wind balance response to the increase in the equator-to-pole temperature gradient at upper levels, itself a consequence of enhanced warming in the middle and upper tropical troposphere and less warming in the upper troposphere at higher latitudes (Rind 2008). Given that the structure and amplitude of stationary waves is very dependent on the strength of the jet stream, changes in zonal and meridional winds are strongly related. The pattern of change in upper-tropospheric meridional winds can be understood from simple theoretical arguments (Simpson et al. 2016). Linear theory of barotropic Rossby waves on a zonal-mean zonal flow u_0 away from sources states that the total wavenumber for stationary waves is given by

$$K = \sqrt{k^2 + l^2} = \sqrt{\frac{\beta - \frac{\partial^2 u_0}{\partial y^2}}{u_0}}, \tag{1}$$

where k and l are the zonal and meridional wavenumber, respectively (e.g., Hoskins and Ambrizzi 1993). In the current climate, stationary waves with nondimensional zonal wavenumbers smaller than 7 are largely prevalent (Simpson et al. 2016). As u_0 increases, K must decrease. Assuming unchanged l, the zonal wavenumber must also decrease, which leads to an increase in the wavelength of stationary waves. Because the wave sources are mainly tied to Earth's topography and are therefore largely fixed in space, the change in wavenumber translates into a phase change downstream from sources, where stationary waves extend further eastward in future climate projections (Fig. 2a).

Upper-tropospheric meridional wind changes are somewhat stronger and more robust over North America than the Mediterranean, yet overall the magnitude of meridional wind changes is rather uniform across longitudes (Fig. 2b). A direct consequence of the eastward shift is the development of an anomalous upper-level anticyclonic circulation over the Mediterranean. This anomalous pattern is also expected at lower levels due to the generally equivalent barotropic nature of winter stationary waves (Held et al. 1985, 2002). The wavelike pattern is indeed still present at the 850-hPa level but does not follow a simple dampening of the 300-hPa pattern. The largest circulation changes are now found over the Mediterranean and off the western coast of North America, whereas meridional wind anomalies are quite weak over the tropical Atlantic, the Gulf of Mexico, and the Arabian Peninsula. While there is clearly an overall equivalent

barotropic structure over the North Atlantic, Pacific and the Mediterranean, the pattern appears more baroclinic over Asia and North America.

Significant longitudinal variations in the vertical structure of Northern Hemisphere winter circulation have been documented by Blackmon et al. (1979). They found that over the central and eastern parts of the Atlantic and Pacific oceans, and Western Europe, the vertical mode is highly barotropic with strong vertical coherence. On the other hand, North America and Asia are characterized by a more baroclinic structure with little coherence between low- and upper-level fluctuations. It follows from this observation that lower-tropospheric flow over the large continental masses should be much less sensitive to stationary circulation changes than over oceans, which is consistent with the comparison between 300- and 850-hPa meridional wind changes. To find the physical cause of this empirical finding, we turn to linear theory of midlatitude dynamics.

b. The external mode

For atmospheric conditions typically prevailing in the midlatitudes, there exists a single trapped vertical mode for Rossby waves propagating on a mean westerly zonal flow with vertical shear, referred to as the external mode (Held et al. 1985). Since this mode therefore connects the upper- and lower-tropospheric circulation, differences in the surface response to similar high-level circulation anomalies should be partly related to variability in the external mode itself. A lack of vertical coherence of the stationary circulation could also locally relate to vertically propagating Rossby waves over regions of topography, but here we focus on the structure of the external mode since it should be an important factor over all land regions as well as over ocean.

The vertical structure of the external mode can be calculated by solving the stationary quasigeostrophic potential vorticity and thermodynamic equations on a beta-plane of infinite zonal extent, linearized about a mean zonal flow $\overline{u}(p)$ between the surface and the 50-hPa level:

$$\frac{\partial q}{\partial t} + \overline{u}\frac{\partial q}{\partial x} + \frac{\partial \psi}{\partial x}\left[\beta - \frac{\partial}{\partial p}\left(\frac{f^2}{\sigma}\frac{d\overline{u}}{dp}\right)\right] = 0, \tag{2}$$

where

$$q = \Delta\psi + \frac{\partial}{\partial p}\left(\frac{f^2}{\sigma}\frac{\partial \psi}{\partial p}\right)$$

is the anomalous quasigeostrophic potential vorticity, ψ is the anomalous streamfunction, f is the Coriolis parameter, β is its meridional gradient, $\omega = Dp/Dt$, and

$$\sigma = -\frac{RT}{p}\frac{d\log(\theta)}{dp}$$

is the static stability parameter. At the surface and at 50 hPa, we obtain boundary conditions from the thermodynamic equation

$$\left(\frac{\partial}{\partial t} + \overline{u}\frac{\partial}{\partial x}\right)\frac{\partial \psi}{\partial p} - \frac{\partial \psi}{\partial x}\frac{d\overline{u}}{dp} = -\frac{\sigma\omega}{f} \tag{3}$$

by enforcing $\omega = 0$. In looking for stationary solutions of the form $\psi(x, y, p) = \mathrm{Re}[\hat{\psi}(p)e^{i(kx+ly)}]$, Eq. (2) becomes

$$\frac{1}{\overline{u}}(\overline{u}\Gamma + \beta - \Gamma\overline{u})\hat{\psi} = K^2\hat{\psi}, \tag{4}$$

where

$$\Gamma = \frac{\partial}{\partial p}\left(\frac{f^2}{\sigma}\frac{\partial}{\partial p}\right)$$

and $K^2 = k^2 + l^2$, and Eq. (3) becomes

$$\overline{u}\frac{d\hat{\psi}}{dp} = \frac{d\overline{u}}{dp}\hat{\psi}. \tag{5}$$

Equations (4) and (5) form an eigenvalue problem with eigenvalue K^2, and the eigenvector associated with the most positive eigenvalue corresponds to the external mode. Solutions to Eqs. (4) and (5) are computed numerically using centered finite differences in pressure. We checked that a single positive mode ($K > 0$) was always found, although setting the lid at a higher level (pressure below 50 hPa) sometimes yields additional spurious modes as discussed in Held et al. (1985). We normalize the external mode by its value at 300 hPa, which is usually close to the maximum.

The external mode is conventionally computed at a given latitude from zonal- and time-mean wind and temperature data (Held et al. 1985). Here, however, we are particularly interested in the variability of the external mode with longitude, and as noted in the introduction to Held et al. (1985) it is possible to define a zonally localized external mode if the time-mean flow is sufficiently slowly varying in longitude. Therefore, we calculate the December–February external mode along the 40°N latitude circle, for ERA-Interim data and each CMIP5/AMIP model in all scenarios, by averaging atmospheric data between 35° and 45°N and then taking a running mean over 60° longitude intervals. We choose a 60° width as a compromise between a width large enough to correctly represent the mean state across the stationary wavelength that dominates the climate change response (waves with nondimensional zonal wavenumber 5 account for most of the projected 300-hPa meridional wind change; Simpson et al. 2016) and a width small enough to capture zonal variability in the mean state. Subsurface values are discarded based on each model's mean surface pressure; for each 60° interval, the surface level used in Eq. (4) is chosen as the highest pressure level with at least 50% of valid data. We refer to the zonally varying external mode as $\hat{\psi}(p, \lambda)$, where λ is longitude. For comparison, we also calculate the external mode using zonally averaged fields and refer to it as $\hat{\psi}_0(p)$.

The external mode allows us to estimate the near-surface component of the stationary wave response using only as input the flow response in the upper troposphere. We compute estimates of the 850-hPa meridional wind change at 40°N

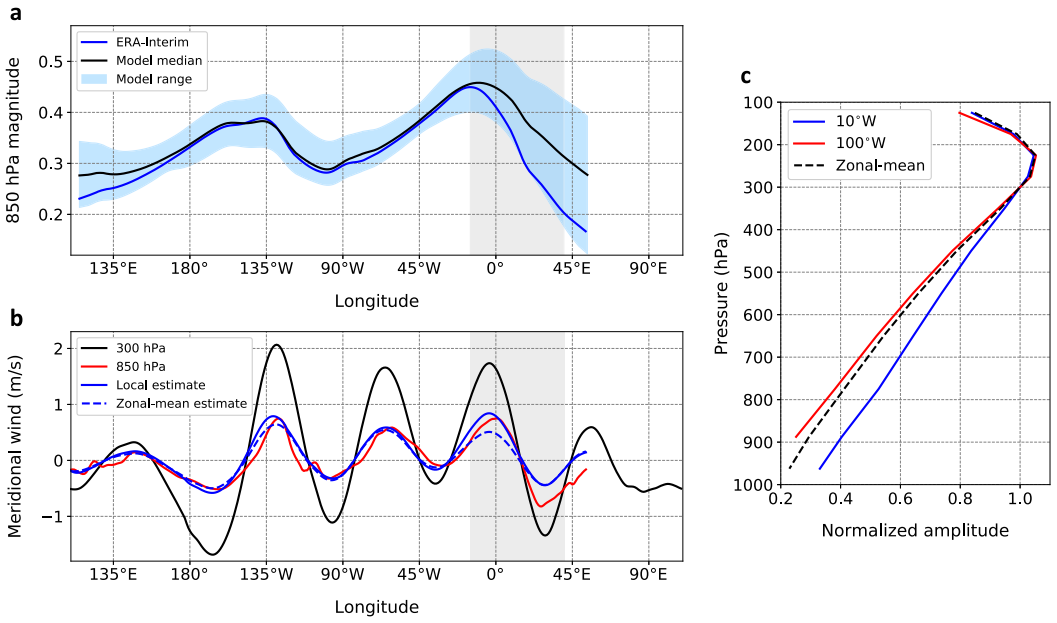

FIG. 3. (a) Value of the DJF external mode at 850 hPa and 40°N as a function of longitude: CMIP5 median in the historical (1976–2005) scenario (black), 95% range (light-blue shading), and ERA-Interim (blue; calculated with 1979–2018 data). The external mode is normalized so that it is equal to 1 at 300 hPa. (b) CMIP5 multimodel mean DJF meridional wind change (35°–45°N average) at 300 (black) and 850 (red) hPa, the estimate based on the external-mode structure (solid blue), and the estimate based on the zonal-mean external mode (dashed blue). In (a) and (b), the Mediterranean region (15°W–40°E) is highlighted in light gray. (c) Examples of external-mode calculations in ERA-Interim at 10°W (blue), at 100°W (red), and with zonal-mean data (dashed black).

(35°–45°N average) in the RCP8.5 (for CMIP) and "amipFuture" (for AMIP) scenarios by multiplying, at each longitude, the mean 300-hPa meridional wind by the external-mode component at 850 hPa (recalling that the external mode is normalized to be 1 at 300 hPa) and taking the difference between the two scenarios. So, for CMIP models, this corresponds to

$$\Delta v^{850}_{\text{est}}(\lambda) = \hat{\psi}^{850}_{\text{RCP8.5}}(\lambda) v^{300}_{\text{RCP8.5}}(\lambda) - \hat{\psi}^{850}_{\text{hist}}(\lambda) v^{300}_{\text{hist}}(\lambda), \qquad (6)$$

where historical values are averaged over the 1976–2005 period and RCP8.5 values over the 2071–2100 period. Using only the historical external mode leads to local differences of less than 5%, and therefore differences in external-mode amplitudes between scenarios is of minor importance in our problem.

c. *Results*

Zonal variability of the external mode is shown on Fig. 3a. Consistent with the findings of Blackmon et al. (1979), the structure of the external mode exhibits a substantial zonal variability. Eastern ocean basins and western continental margins are characterized by much stronger vertical coherence, with larger amplitudes in the lower troposphere, than continents. In particular, the external-mode amplitude at 850 hPa is maximal over the western Mediterranean (≈0.43 when averaged over 10°W–0° in ERA-Interim). Over western North America (125°–115°W), that amplitude is only 0.32. The ERA-Interim reference external mode is calculated over a time period (1979–2018) that is different from that of CMIP5 models (1976–2005), but results are the same when considering a shorter time period (e.g., 1979–2005) for ERA-Interim data.

The variations with longitude in Fig. 3a essentially reflect the variability in the vertical structure of the zonal wind profile. Indeed, estimates of the vertical mode based on zonal-mean static stability values show little difference with the Fig. 3a values. The external mode tends to have similar vertical structure as the mean zonal wind (Held et al. 2002) (Fig. 3c), and thus the external mode is more barotropic the smaller the vertical shear of the mean zonal wind. This vertical shear is strongest on the western side of ocean basins and adjacent land in the storm track entrance regions (corresponding to a weak external mode at 850 hPa) and weakest on the eastern side of ocean basins and adjacent land (corresponding to a strong external mode at 850 hPa). Differences in friction between land and ocean can also affect the vertical structure of the mean zonal wind and thus the zonal variability of the external mode. In particular, the Mediterranean has relatively weak wind shear and a strong external mode at 850 hPa since in winter it typically lies to the east of the North Atlantic jet and to the north of the subtropical jet over Africa [see e.g., Fig. 1b of Harnik et al. (2014)]. In the Pacific storm track, between 135°E and 135°W, large 300-hPa winds and weak near-surface winds generate strong shear, resulting in a smaller 850-hPa external-mode magnitude relative to the North Atlantic.

It is interesting to notice from Fig. 3a, however, that although the external-mode amplitude is generally well-reproduced in

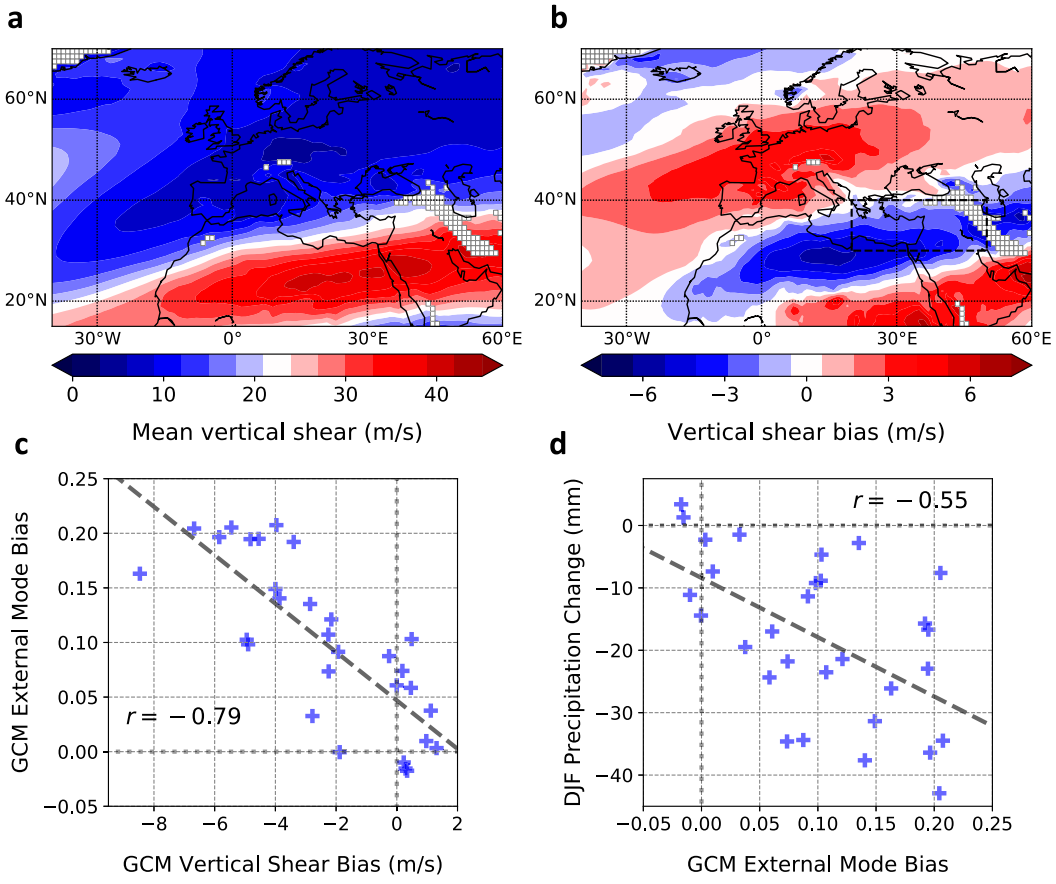

FIG. 4. (a) DJF Mediterranean mean vertical wind shear, from ERA-Interim. (b) CMIP5 multimodel-mean bias in DJF Mediterranean vertical wind shear. (c) Bias in vertical wind shear over the southeastern Mediterranean region [30°–40°N, 20°–50°E; see dash-outlined rectangle in (b)] against bias in the eastern Mediterranean (16°–46°E) external-mode magnitude at 40°N across CMIP5 models. The region for wind shear calculation is selected empirically on the basis of its high correlation with the eastern Mediterranean external-mode bias. (d) Bias in 850-hPa external-mode amplitude over the southeastern Mediterranean region [as in (c)] against Mediterranean (30°–45°N, 10°W–40°E) precipitation change under RCP8.5. In (a)–(c), vertical wind shear is defined as 300-hPa zonal wind minus 850-hPa zonal wind. In (c) and (d), best-fit linear regression lines are shown in dashed black.

models, across the 40°N latitude circle, the single area of significant discrepancy is the central and eastern Mediterranean, up to the beginning of the Central Asian mountain chains (10°–55°E). There, models almost systematically overestimate the low-level external-mode amplitude, on average by 40%. This suggests that, even if the upper-level circulation change projected by models is realized, the regional surface circulation response will be weaker than in model projections. In addition, intermodel scatter in external-mode magnitude in this region is much larger than elsewhere, which may point to differences in the resolution of orography and in the effect of orography on the large-scale flow. The overestimation of the external-mode component over the eastern Mediterranean seems related to a large underestimation of zonal wind shear by GCMs over northern Africa and the Middle East, along the northern border of the North African jet (Fig. 4). Weaker shear is consistent with an overestimation of external-mode magnitude at low levels, although biases in mean 300-hPa zonal wind may also matter [see Eq. (4)]. In addition, Fig. 4 also shows that CMIP5 models tend to overestimate vertical shear in the North Atlantic midlatitude jet over northwestern Europe, consistent with their average bias toward a too zonal storm track during winter (Simpson et al. 2020). The bias of too little shear further south may be related to a bias of of the jet being too rarely in its southward position (Simpson et al. 2020), though a comprehensive analysis of circulation biases over Europe would be required.

This zonal variability has important implications for the low-level circulation response. Figure 3b shows the two estimates of the 850-hPa meridional wind change, using either the zonally varying or the constant external mode, averaged across all models. In general, the two estimates are very consistent with the 300-hPa model response. The magnitude of the 850-hPa change is correctly captured, even with the zonal-mean external mode, except where the external-mode amplitude reaches a local maximum, i.e., over the western Mediterranean (≈10°W)

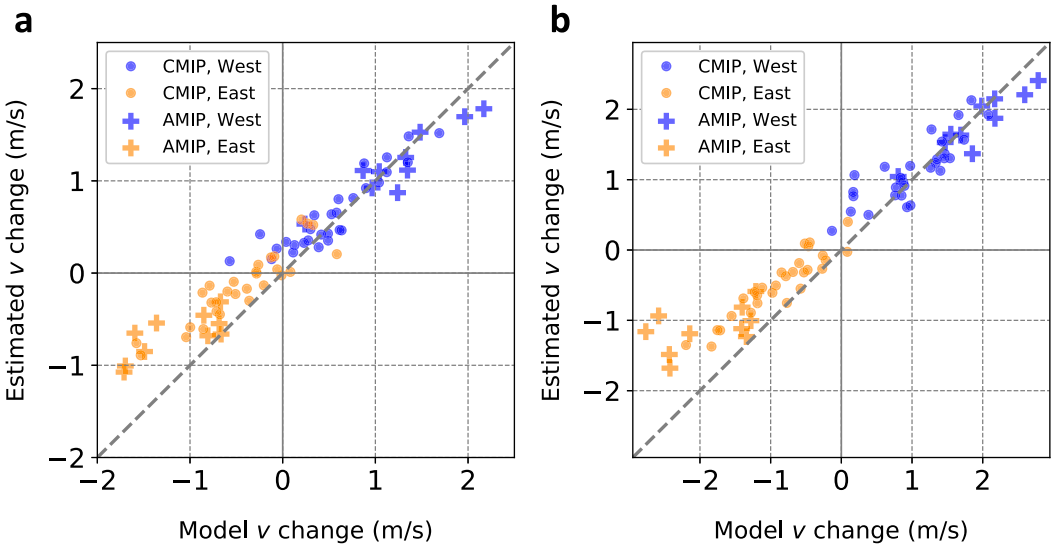

FIG. 5. The 850-hPa meridional wind change (35°–45°N average) in the western (15°W–15°E; blue) and eastern (16°–46°E; orange) Mediterranean in CMIP5 (circles) and AMIP (crosses) models. The changes estimated through the external mode [Eq. (6)] are plotted vs the changes in the models. Shown are (a) changes averaged over each region and (b) the maximum changes in each region.

and off the coast of Western North America (≈135°W). Over each of these regions, the peak in 850-hPa external-mode amplitude coincides with a peak in 300-hPa meridional wind change, so that important discrepancies are found between the zonal- and local-based meridional wind estimates. In the western Mediterranean in particular, it is necessary to use the local external-mode value to account for the full magnitude of the 850-hPa wind change.

It is important to point out that the estimate based on Eq. (6) does not explicitly take the potential vertical tilt of the stationary circulation into account. A small phase shift can indeed be detected on Fig. 3b between the 850-hPa response and its external-mode-based estimate, for instance between 90° and 30°W, that could be related to vertical tilt in the time-mean circulation. However, the magnitude of the 850-hPa response is still correctly estimated. Our argument is therefore still valid, even if for an accurate estimate of the low-level response at a given longitude, one should also take into account any tilts in the circulation.

It must also be stressed that the local external mode only gives information about the local vertical structure of the time-mean circulation. Therefore, in the climate change context, this approach can only give information about zonal variability in the vertical structure of the circulation response, not zonal variability in the circulation response itself. In particular, the circulation estimate from Eq. (6) relies on taking the 300-hPa response in CMIP5 models as given. Future work should focus on providing a theoretical understanding, for instance with a stationary wave model in an idealized setting, on the extent to which zonal variations in the local external mode can lead to variations in the amplitude of the stationary wave in the upper troposphere (e.g., at 300 hPa) in addition to variations near the surface.

In addition to the multimodel mean, intermodel spread is also well explained by this approach. Figure 5 shows the values of the local external-mode-based estimate of 850-hPa wind change against those given by models. We consider both the average and the maximum change. There is excellent agreement in both cases, although for models falling at the extremes the external-mode-based estimate tends to underestimate the wind response, particularly in the eastern Mediterranean. The larger changes found in the AMIP simulations are also well accounted for by this method, i.e., they mainly result from larger circulation changes in the upper troposphere in AMIP simulations. Differences in external-mode magnitude across models are found to play a smaller role in the spread of 850-hPa meridional wind projections when compared with the scatter in upper-tropospheric trends.

Since precipitation projections for the Mediterranean are strongly related to the strength of low-level circulation changes (Zappa and Shepherd 2017, TE20), the external-mode approach can also account for intermodel spread in precipitation trends. Additionally, for a given 300-hPa response, a larger external-mode amplitude over the Mediterranean will translate into larger low-level circulation changes. It is therefore interesting to test whether CMIP5 GCM biases in external-mode amplitude and vertical wind shear are linked to the magnitude of precipitation projections in the Mediterranean. Figure 4d shows that it is indeed the case: larger external-mode biases over the eastern Mediterranean tend to be associated with more severe declines in winter precipitation. There is naturally a substantial spread, given that the strength of the 300-hPa response is not fixed for a given shear bias. Still, the relationship is significant (p value < 0.05) and relies on a clear physical mechanism. Therefore, biases in shear across climate models can be seen as an emergent constraint (Hall et al. 2019)

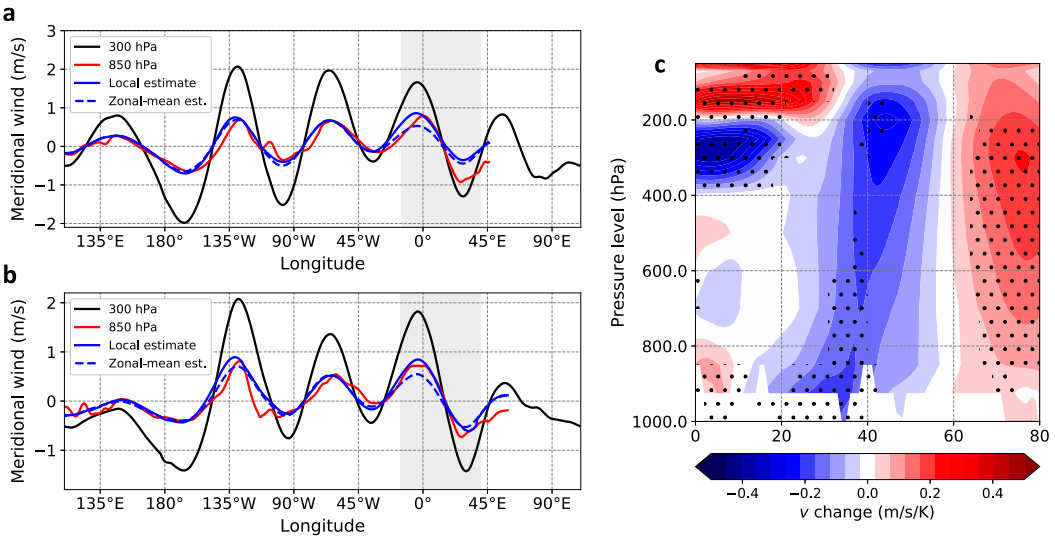

FIG. 6. CMIP5 multimodel mean DJF meridional wind change averaged over (a) 35°–40°N and (b) 40°–45°N, at 300 (black) and 850 (red) hPa, the estimate based on the external-mode structure (solid blue), and the estimate based on the zonal-mean external mode (dashed blue). In (a) and (b), the Mediterranean region (15°W–40°E) is highlighted in light gray. (c) CMIP5 multimodel mean change in meridional wind averaged over 16°–46°E under RCP8.5 (2071–2100 minus 1976–2005), normalized by each model's global-mean temperature change. Stippling indicates that 80% or more of models agree on the sign of the change.

to reduce the spread in future Mediterranean precipitation trends during winter.

Although the GCMs tend to overestimate the barotropicity of the circulation over the eastern Mediterranean, it is also clear from Fig. 3b that in that region, both external-mode-based meridional wind estimates account for only half or so of the observed wind change in models (the difference is, on average, 0.3 m s^{-1}). To test whether this conclusion is sensitive to our choice of central latitude, we repeat the external-mode analysis over 5° latitude bands centered at 37.5° and 42.5°N. Results in Figs. 6a and 6b show that while the external-mode approach accounts for much of the 850-hPa meridional wind response over 40°–45°N, it largely underestimates it between 35° and 40°N, explaining the original bias identified in Fig. 3b over the full 35°–45°N interval. For further understanding, we consider the vertical structure in the zonally averaged meridional wind change over the eastern Mediterranean (Fig. 6c). Meridional wind trends are largest in magnitude in the upper troposphere, near 200 hPa, where they show a pronounced decline around 45°N consistent with Fig. 2b. The amplitude of the trends decreases with pressure, but not all the way to the surface. Rather, a robust secondary local maximum in meridional wind change can be found at the surface, near 35°N. This points to the existence of an additional forcing at the surface, discussed in the next section, that enhances the circulation response linked to upper-tropospheric trends and that can explain the discrepancy between the model and estimated wind responses in Figs. 3 and 6a.

4. Regional circulation response to surface forcing

In addition to upper-tropospheric circulation trends and their impact over the Mediterranean, the regional circulation also responds to the weaker rate of warming of Mediterranean SSTs compared to land, a robust feature over oceans under global warming (Sutton et al. 2007; Byrne and O'Gorman 2018). TE20 argued, based on regional simulations, that in the Mediterranean in winter, the relative cold SST anomaly due to enhanced land warming triggers a regional circulation response with higher pressure downstream of the anomaly and anomalous northeasterlies in the eastern Mediterranean. However, GCM projections for summer clearly show a robust decrease rather than an increase in Mediterranean sea level pressure (Giorgi and Lionello 2008), even though the relative SST cooling is still present in this season. This raises the question of why the winter circulation might be more sensitive to surface thermodynamic forcing than the summer one. We now revisit the simulations of TE20 to look for an explanation and to discuss how the relative SST cooling relates to the inability of the external-mode argument to explain the full response in the eastern Mediterranean.

Figure 7 shows the mean 850-hPa geopotential height and wind difference between the perturbed ("+1.5°C") and the reference ("0°C") simulations (which represents the impact of the relative sea cooling) for winter [December–February (DJF)] and summer [June–August (JJA)], averaged for the two sets of simulations (ERA and MPI). First, the winter circulation response to relative SST cooling is evidently much larger than the summer one: though geopotential height tends to increase in both seasons, the increase during winter is about 3.5 times that during summer (Figs. 7a and 7c). Additionally, the winter response consists of a well-defined anticyclonic anomaly centered south of Greece, while in summer, the geopotential height change exhibits a more uniform increase over the Mediterranean. The associated summer circulation response is small everywhere ($\leq$0.1 m s^{-1}).

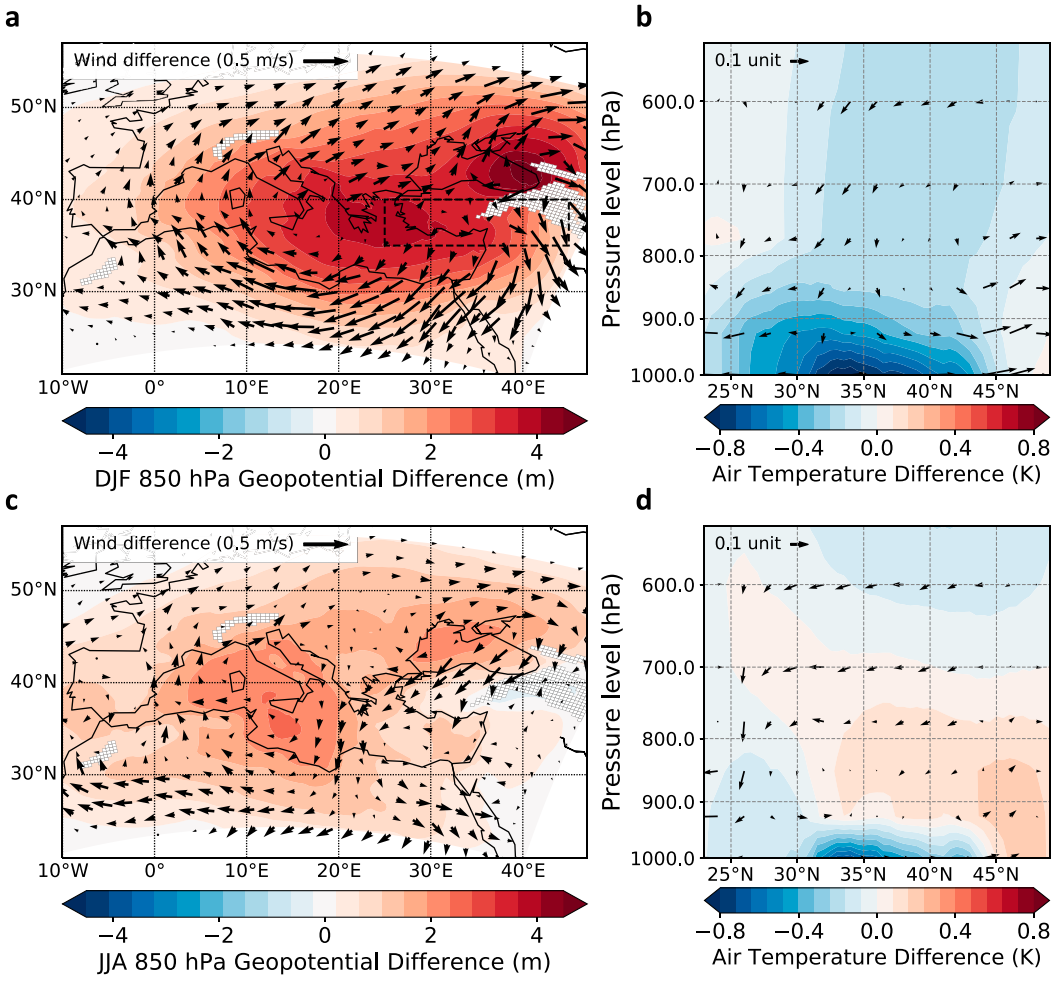

FIG. 7. Difference in (a),(c) 850-hPa geopotential height and wind and (b),(d) zonally averaged (0°–40°E) air temperature, meridional wind, and pressure velocity, between the "0C" and "+1.5C" simulations ("0C" minus "+1.5C"; average of ERA and MPI runs) for (top) winter (DJF) and (bottom) summer (JJA). In (b) and (d), circulation vectors are scaled such that 1 horizontal unit = 1 m s^{-1} and 1 vertical unit = 0.2 hPa h^{-1}.

For further analysis, we look at the temperature and circulation response on pressure levels (Figs. 7b,d). The striking difference is that during winter, the relative cooling extends much higher into the lower troposphere (up to 850 hPa, and even weakly above that) than in summer, when it is confined to the very lowest model level. As expected, there is little to no circulation response below 800 hPa in summer, whereas at these levels in winter there is noticeable divergence and weak descent.

To determine why the winter circulation is more sensitive to relative SST cooling, we now turn to near-surface static stability σ. Its annual cycle at 925 hPa averaged over the Mediterranean Sea is shown on Figs. 8a. There is a strong winter/summer contrast, with static stability that is 2 times as large in summer as in winter. This seasonal contrast is consistent with the smaller amplitude of the annual cycle of SSTs compared to low-level air temperature. In winter, SSTs and near-surface air are warmer than overlying air layers, which is conducive to low static stability, while in summer the situation is reversed: relatively warmer low-level air temperatures are associated with enhanced static stability. The large summer static stability prevents communication of the relative cooling to levels higher than the near surface.

It is important to put this analysis in the context of the regional circulation. The regional circulation is dominated during summer by the large-scale descent forced by the Indian monsoon to the east (Rodwell and Hoskins 1996), which contributes to enhanced static stability of the air column. There is no such forced signal during winter: the area of strong descent near the regional Hadley cell edge is over the Sahara Desert, well to the south of the Mediterranean (Fig. 9). Therefore, the Mediterranean Sea is located enough to the north of the Hadley cell such that the warm SSTs can trigger large-scale ascent over the sea, a striking feature of the vertical circulation (Fig. 9a). This large-scale ascent in turns helps propagate the cooling anomaly upward into the troposphere in

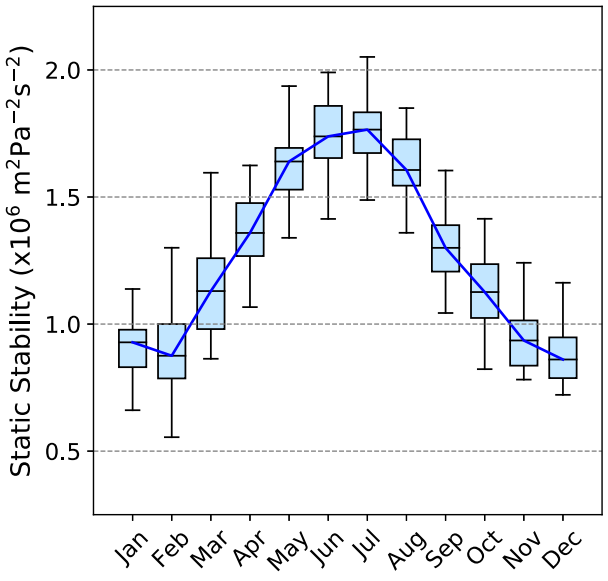

FIG. 8. Annual cycle of 925-hPa Mediterranean-average (30°–45°N, 10°W–45°E) static stability, from ERA-Interim (1979–2018). Boxes represent the 50% range over the 40 years of data, and whiskers show the full range.

our simulations, whereas it remains confined near the surface during summer (Figs. 7b,d). The combination of the descent and large static stability in summer explains why there is no associated anomalous circulation above the surface since there is no heating anomaly to compensate (Hoskins and Karoly 1981).

In our simulations, the winter relative SST cooling leads to an anomalous high pressure that is centered to the south and east of the anomalous high in the mulimodel CMIP5 simulations (cf. Fig. 1a with Fig. 7a). There are strong anomalous northerlies to the east of the basin, around 30°–35°N (Fig. 7a). To the west, the meridional wind response is weaker, consistent with the fact that the stationary wave response explains almost all of the magnitude in meridional wind trends west of 15°E (Fig. 3b). Thus, the surface forcing helps to explain the inability of the external-mode estimate to account for the full 850-hPa meridional wind response in GCMs around 35°N. The difference in the eastern Mediterranean between projected and estimated meridional wind responses in the 35°–40°N band is concentrated between 25° and 45°E (Fig. 6b), where it averages $-0.5\,\mathrm{m\,s^{-1}}$. Within that same area (35°–40°N, 25°–45°E; see rectangle in Fig. 7a), the MRCM experiments indicate a $-0.23\,\mathrm{m\,s^{-1}}$ average wind change in response to the surface forcing. This suggests that simply adding the two mechanisms may not be sufficient to explain the total circulation response at 40°N. A nonlinear superposition of the dynamical responses to each forcing may explain part of that discrepancy (TE20). That superposition is made more complex by the difference in the latitudes of maximum upper-tropospheric (45°N) and surface forcing (30°N), which leads to a noticeable vertical tilt in the meridional wind change (Fig. 6c). Additionally, the use of a different modeling framework, the finer representation of topography, the influence of friction and high topography on the mean circulation (Simpson et al. 2015) all possibly contribute to shaping the low-level circulation response. Further investigation is warranted, particularly since GCMs probably overestimate the dynamical response to upper-level forcing in the first place, because of their bias in

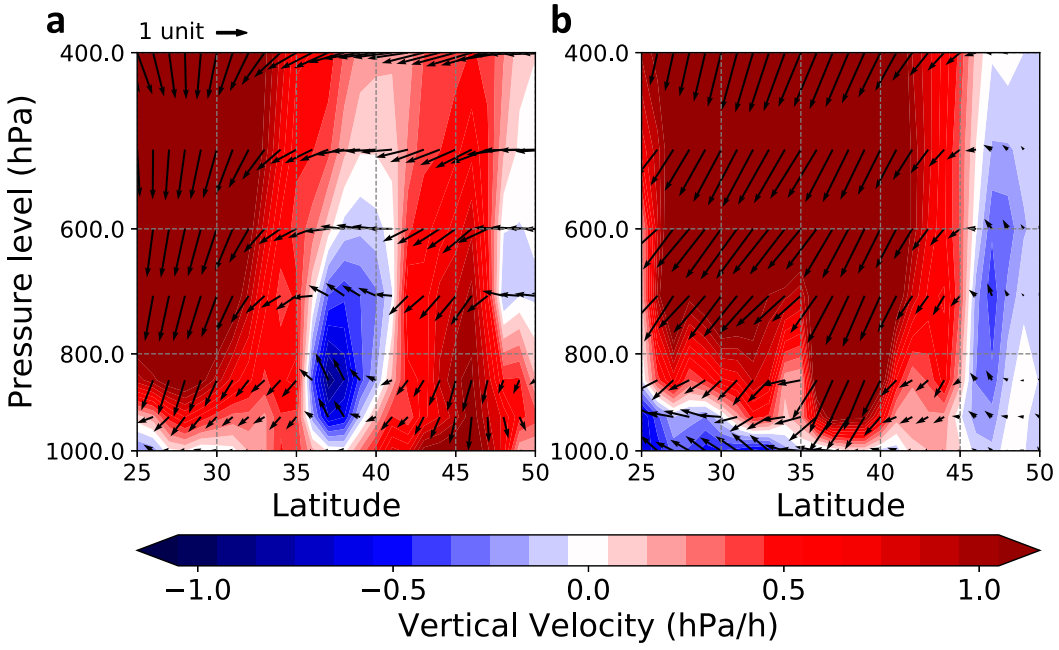

FIG. 9. Mediterranean (10°W–45°E) zonal-mean (a) DJF and (b) JJA vertical and meridional circulation: vertical velocity (color shades) and wind in the meridional-pressure plane (arrows), in ERA-Interim (1979–2018). Circulation vectors are scaled such that 1 horizontal unit = $3\,\mathrm{m\,s^{-1}}$ and 1 vertical unit = $1\,\mathrm{hPa\,h^{-1}}$.

external-mode magnitude over the eastern Mediterranean (Figs. 3a and 4c,d).

5. Conclusions

We set out to explain the dynamics of two important aspects of Mediterranean circulation trends in a warming climate: why the region experiences in winter a larger surface stationary wave response compared to other regions at a similar latitude, and why the response to relative SST cooling is much larger in winter than summer. First, the Mediterranean during winter is characterized by relatively weak vertical shear in the mean zonal wind, being situated to the east of the North Atlantic jet and to the north of the subtropical jet over Africa. This weak vertical shear imprints on a local external mode (defined over 60° in longitude) and makes the stationary wave response in this region relatively barotropic. As a result, the low-level circulation is particularly sensitive to changes in the stationary wave pattern, leading to a pronounced anticyclonic anomaly. Second, although the relative SST cooling is a year-round feature, its dynamical impact is strongly modulated by the large seasonal variations in low-level static stability and the background circulation. Low static stability during winter allows the heating anomaly to propagate from the surface into the lower troposphere and trigger a circulation response, while in summer, high static stability and intense descent forced by the Indian monsoon keep the heating anomaly confined to the surface.

The physical mechanisms behind wintertime Mediterranean climate projections are robust, but there remains high intermodel uncertainty in the low-level circulation response, and our results show this is mostly linked to differences in the upper-level circulation response. The upper-level circulation response has in turn been related to changes in stationary wave propagation (Simpson et al. 2016), and a deeper understanding of these changes will be required to reduce the uncertainty in Mediterranean projections. In particular, determining what controls the amplitude of the stationary circulation response across GCMs and whether it may be affected by biases in the historical circulation remain open questions. Importantly, we find that the low-level regional circulation response connected to stationary wave shifts may be overestimated in GCMs because their external-mode magnitude over the eastern Mediterranean is larger than in ERA-Interim. This bias is related to models underestimating vertical wind shear over the eastern Mediterranean, and it is related through an emergent constraint to the future precipitation response for the whole Mediterranean (Fig. 4d), suggesting that Mediterranean wintertime circulation change, and consequently precipitation decline, may be overestimated by GCMs.

Acknowledgments. We acknowledge the World Climate Research Programme's Working Group on Coupled Modelling, which is responsible for CMIP, and we thank the climate modeling groups for producing and making available their model output. This work was made possible through funding from the Office Chérifien des Phosphates (OCP) through Université Mohamed VI Polytechnique, Morocco.

Data availability statement. ERA-Interim reanalysis data are available from 1979 to 2019 (https://apps.ecmwf.int/datasets/data/). CMIP and AMIP model output were downloaded from https://esgf-index1.ceda.ac.uk/projects/esgf-ceda/. Regional simulations are available upon request to the corresponding author.

REFERENCES

Blackmon, M. L., R. A. Madden, J. M. Wallace, and D. S. Gutzler, 1979: Geographical variations in the vertical structure of geopotential height fluctuations. *J. Atmos. Sci.*, **36**, 2450–2466, https://doi.org/10.1175/1520-0469(1979)036<2450:GVITVS>2.0.CO;2.

Brogli, R., S. Sørland, N. Kröner, and C. Schär, 2019: Causes of future Mediterranean precipitation decline depend on the season. *Environ. Res. Lett.*, **14**, 114017, https://doi.org/10.1088/1748-9326/ab4438.

Byrne, M. P., and P. O'Gorman, 2018: Trends in continental temperature and humidity directly linked to ocean warming. *Proc. Natl. Acad. Sci. USA*, **115**, 4863–4868, https://doi.org/10.1073/pnas.1722312115.

Dee, D. P., and Coauthors, 2011: The ERA-Interim reanalysis: Configuration and performance of the data assimilation system. *Quart. J. Roy. Meteor. Soc.*, **137**, 553–597, https://doi.org/10.1002/qj.828.

Gates, W., and Coauthors, 1999: An overview of the results of the Atmospheric Model Intercomparison Project (AMIP I). *Bull. Amer. Meteor. Soc.*, **80**, 29–55, https://doi.org/10.1175/1520-0477(1999)080<0029:AOOTRO>2.0.CO;2.

Giorgi, F., and P. Lionello, 2008: Climate change projections for the Mediterranean region. *Global Planet. Change*, **63**, 90–104, https://doi.org/10.1016/j.gloplacha.2007.09.005.

Hall, A., P. Cox, C. Huntingford, and S. Klein, 2019: Progressing emergent constraints on future climate change. *Nat. Climate Change*, **9**, 269–278, https://doi.org/10.1038/s41558-019-0436-6.

Harnik, N., E. Galanti, O. Martius, and O. Adam, 2014: The anomalous merging of the African and North Atlantic jet streams during the Northern Hemisphere winter of 2010. *J. Climate*, **27**, 7319–7334, https://doi.org/10.1175/JCLI-D-13-00531.1.

Held, I. M., R. Panetta, and R. Pierrehumbert, 1985: Stationary external Rossby waves in vertical shear. *J. Atmos. Sci.*, **42**, 865–883, https://doi.org/10.1175/1520-0469(1985)042<0865:SERWIV>2.0.CO;2.

——, M. Ting, and H. Wang, 2002: Northern winter stationary waves: Theory and modeling. *J. Climate*, **15**, 2125–2144, https://doi.org/10.1175/1520-0442(2002)015<2125:NWSWTA>2.0.CO;2.

Hoskins, B. J., and D. J. Karoly, 1981: The steady linear response of a spherical atmosphere to thermal and orographic forcing. *J. Atmos. Sci.*, **38**, 1179–1196, https://doi.org/10.1175/1520-0469(1981)038<1179:TSLROA>2.0.CO;2.

——, and T. Ambrizzi, 1993: Rossby wave propagation on a realistic longitudinally varying flow. *J. Atmos. Sci.*, **50**, 1661–1671, https://doi.org/10.1175/1520-0469(1993)050<1661:RWPOAR>2.0.CO;2.

Rind, D., 2008: The consequences of not knowing low- and high-latitude climate sensitivity. *Bull. Amer. Meteor. Soc.*, **89**, 855–864, https://doi.org/10.1175/2007BAMS2520.1.

Rodwell, M. J., and B. J. Hoskins, 1996: Monsoons and the dynamics of deserts. *Quart. J. Roy. Meteor. Soc.*, **122**, 1385–1404, https://doi.org/10.1002/qj.49712253408.

Seager, R., H. Liu, N. Henderson, I. R. Simpson, C. Kelley, T. Shaw, Y. Kushnir, and M. Ting, 2014: Causes of increasing aridification of the Mediterranean region in response to rising greenhouse gases. *J. Climate*, **27**, 4655–4676, https://doi.org/10.1175/JCLI-D-13-00446.1.

——, T. Osborn, Y. Kushnir, I. Simpson, J. Nakamura, and H. Liu, 2019: Climate variability and change of Mediterranean-type climates. *J. Climate*, **32**, 2887–2915, https://doi.org/10.1175/JCLI-D-18-0472.1.

Simpson, I. R., R. Seager, T. Shaw, and M. Ting, 2015: Mediterranean summer climate and the importance of Middle East topography. *J. Climate*, **28**, 1977–1996, https://doi.org/10.1175/JCLI-D-14-00298.1.

——, ——, M. Ting, and T. Shaw, 2016: Causes of change in Northern Hemisphere winter meridional wind and regional hydroclimate. *Nat. Climate Change*, **6**, 65–70, https://doi.org/10.1038/nclimate2783.

——, and Coauthors, 2020: An evaluation of the large-scale atmospheric circulation and its variability in CESM2 and other CMIP models. *J. Geophys. Res. Atmos.*, **125**, e2020JD032835, https://doi.org/10.1029/2020JD032835.

Sutton, R. T., B. Dong, and J. M. Gregory, 2007: Land/sea warming ratio in response to climate change: IPCC AR4 model results and comparison with observations. *Geophys. Res. Lett.*, **34**, L02701, https://doi.org/10.1029/2006GL028164.

Taylor, K. E., R. J. Stouffer, and G. A. Meehl, 2012: An overview of CMIP5 and the experiment design. *Bull. Amer. Meteor. Soc.*, **93**, 485–498, https://doi.org/10.1175/BAMS-D-11-00094.1.

Tuel, A., and E. Eltahir, 2020: Why is the Mediterranean a climate change hotspot? *J. Climate*, **33**, 5829–5843, https://doi.org/10.1175/JCLI-D-19-0910.1.

Wills, R. C. J., R. H. White, and X. J. Levine, 2019: Northern Hemisphere stationary waves in a changing climate. *Curr. Climate Change Rep.*, **5**, 372–389, https://doi.org/10.1007/s40641-019-00147-6.

Zanchettin, D., A. Rubino, D. Matei, O. Bothe, and J. Jungclaus, 2013: Multidecadal-to-centennial SST variability in the MPI-ESM simulation ensemble for the last millennium. *Climate Dyn.*, **40**, 1301–1318, https://doi.org/10.1007/s00382-012-1361-9.

Zappa, G., and T. G. Shepherd, 2017: Storylines of atmospheric circulation change for European regional climate impact assessment. *J. Climate*, **30**, 6561–6577, https://doi.org/10.1175/JCLI-D-16-0807.1.

——, B. J. Hoskins, and T. G. Shepherd, 2015: The dependence of wintertime Mediterranean precipitation on the atmospheric circulation response to climate change. *Environ. Res. Lett.*, **10**, 104012, https://doi.org/10.1088/1748-9326/10/10/104012.